Galaxy Voids in Opaque Quasar Sightlines Near the End of Reionization

Azeem Bari

June 8, 2022

Abstract

It is widely assumed that the epoch reionization ended at $z = 6$. However, the quasar ULAS J0148+0600 challenges this assumption given its high opacity trough ($\tau_{eff} \geq 7$). Using Hyper Suprime Cam imaging over six filters, we carried out a survey of LBGs in this field over the redshift interval $5.5 \leq z \leq 5.9$. We found a void of galaxies at this redshift slice, with the most underdense region being within 16' of the quasar. This result is consistent with the deficit of LBGs reported by Kashino et al. (2019), and with the deficit of LAEs at $z = 5.7$ reported in the same field by Becker et al. (2018). This agreement suggests LAEs are reliable for probing density structures surrounding highly opaque sightlines and aren't being suppressed by neutral gas in highly opaque regions. The association of highly opaque sightlines with galaxy underdensities is consistent with models that suggest an ultra-late reionization that has not yet completed by $z = 5.7$.

I Introduction

Due to the extreme temperature and density of the early universe, all of the atoms were ionized, meaning that the protons and electrons were flying around freely, unbounded to each other. This epoch marks the first time the universe was ionized. During this time, the early universe was so hot and dense that nuclear fusion occurred. Protons collided with other protons and overcame the Coulomb repulsion to create primordial hydrogen, helium, and lithium. When protons collide with each other at such high energies, gamma-rays are emitted. Due to the high density of the early universe, the universe itself was opaque to this light. These conditions lasted for hundreds of thousands of years as the universe continued to expand, until it finally became cool and diffuse enough for the ionized hydrogen, helium, and lithium atoms to capture electrons. This process is known as recombination, and it marks the period in which the universe goes from being ionized to electrically neutral. When electrons became bound to the protons, the trapepd photons were finally free and the universe became transparent to light.

Today the intergalactic medium (IGM) is highly ionized. How did it become this way? It should be noted that the universe didn't become reionized at one moment, but rather a process that took many years. First, the universe is full of neutral atoms with the exception of isolated islands of HII (ionized hydrogen) produced from ionizing sources. Secondly, the universe transitions into a phase in which the separate HII regions begin to overlap, but half of the IGM is still neutral. This overlapping continues to happen, leaving only small pockets of neutral gas. Finally, the universe becomes completely ionized as we see it in its present day form (Mo et al. (2010)).

With most of the IGM consisting of hydrogen, studying the Lyman alpha transition is key for understanding reionization. The Lyman alpha transition is seen when an incoming photon is absorbed by a neutral hydrogen atom and excites the electron from the ground state to the first state. These electrons in particular absorb light of the wavelength 121.6 nm, the Lyman alpha line of hydrogen. This, of course, is only the rest wavelength. As the universe expands, shorter wavelengths will get redshifted to the Lyman alpha line, and Lyman alpha lines redshifted to even longer wavelengths.

One of the ways astronomers study reionization is by analyzing spectral lines. For instance, a quasar, a very luminous and distant object, can be used to determine how much neutral hydrogen is still out there. By looking at a its spectrum, one will see a broad emission line produced by the quasar, followed by a series of dips at lower redshifts. Each one of these dips is from a different intergalactic cloud of hydrogen that absorbs the quasar's continuum radiation on its journey to Earth (Carroll and Ostlie (2007)). The lines from the clouds of hydrogen are called absorption lines. A dense thicket of hydrogen absorption lines

is called a Lyman alpha forest. Now, if astronomers were to observe the Lyman alpha forest for a high redshift quasar and see a flattening in its spectrum, we would know that we are observing that quasar during the epoch of reionization. Why is this the case? Well, we know that the universe today is ionized, but during the epoch of reionization, parts of the universe were still neutral. Thus, if there is a flattening in the forest, that would indicate that there is still neutral hydrogen absorbing all of the radiation. This aborsption feature is known as the Gunn-Peterson trough.

The Lyman alpha emission is also very useful for studying galaxies during the epoch of reionization. If the radiation emitted by a galaxy is of wavelength shorter than 912 Å , we expect to see a flattening in its absorption spectrum as well as bluer filters. This is because at higher energies the opacity of the material increases, so the flux decreases. This effect causes a sudden decrease in the flux at a particular wavelength, which is referred to as the Lyman break. The filter in which this break occurs in tells us what range of redshifts the object could be at. This Lyman break method is one way astronomers find galaxies at high redshifts.

There are still many unanswered questions in the field of reionization that merit attention. Most questions regard the duration of this epoch. A study carried out by Fan et al. (2006) suggests reionization ended at $z = 6$. However, a new model of reionization supports late reionization, suggesting that the epoch may have ended later than $z = 6$ Kulkarni et al. (2019). This model would point to large islands of hydrogen in the IGM that remain neutral past $z = 6$. By measuring the quantity of galaxies and the opacity of these islands, we can gauge a better understanding of how reionization works. If a field is highly opaque and shows an underdensity of ionizing sources, it would be consistent with the late reionization scenario. A galaxy survey can be used to trace the underlying density, and the opacity of a sightline can be measured from a quasar's Lyman alpha forest.

Studying the main sources of reionization could prove to be useful for testing late reionization scenarios. These sources of reionization are called Lyman alpha emitters, or LAEs for short. LAEs are young galaxies undergoing a rapid production of star creation, so-called starburst. The ionizing photons emitted by those stars gets absorbed and re-emitted as Lyman alpha (1215.67 Å) by the neutral hydrogen in and around the galaxy. Because of this, they show up really bright in Lyman alpha. Although, these sources may not show up in any of the other bands due to the fact that they're still in the process of making stars and they don't have as much continuum emission.

In this paper, we study the density of Lyman break galaxies in the ULAS J0148+0600 field. A Lyman break galaxy is another type of star forming galaxy with a continuum spectrum that features an absorption trough at wavelengths shorter than 912 Å due to neutral hydrogen, but appear bright at longer wavelengths. This type of galaxy differs from LAEs, which emit only Lyman alpha radiation and can possibly be subject to suppression around highly opaque sightlines. LBGs can be thought of as tracers of the overall density of the universe, because no matter what the most dominant source of ionizing photons is, it will be more plentiful where the universe is dense, as will LBGs. LBG surveys are complementary to LAE surveys as different types of galaxies are used as density tracers. Furthermore, we would like to compare our selection of LBGs with the selection of LAEs presented in Christenson et al. (2021), done in the same field, to determine if there is any relationship in their structures.

We study the J0148 field because it raises questions about when reionization ended. Contrary to the widely believed $z = 6$ ending of reionization, the J0148 sightline suggests that there is an abundance of neutral gas down to z = 5.7, hinting towards late reionization. We summarize the methods used to obtain a catalog of LBG candidates in Section 2, analyze the results and discuss the data in section 3, and summarize in section 4. Throughout this paper, we assume a ΛCDM cosmology with $\Omega_m = 0.3$, $\Omega_\Lambda = 0.7$, and $\Omega_b = 0.048$. All distances are given in comoving units, and all magnitudes are in the AB system.

II Methods

II.I Photometry

The imaging data used for analyzing the quasar field comes from Subaru Hyper Suprime Cam (HSC). The r2, i2, and NB816 measurements were initially taken by Becker et al. (2018). The particular quasar imaged was ULAS J0148+0600 (hereafter J0148). Located at ($z = 6$, R.A. = $01^h48^m37^s.639$, decl.= $+0600'20"01$), J0148 merits its attention due to it's immense (110 h^{-1} Mpc) and opaque ($\tau_{eff} \geq 7$) Lyman-alpha trough (Becker et al. (2015)), one of the most highly opaque sightlines known at this redshift. Moreover, the J0148 field has been reported to have an underdensity of Lyman alpha emitters 20 h^{-1} Mpc of the quasar sightline (Becker et al. (2018), see also Christenson et al. (2021)), further evidence for a potential sce-

nario that ultra-late reionization has not yet concluded at $z = 5.7$. Additionally, a survey done by Kashino et al. (2019) found an underdensity of Lyman break galaxies within a 19 cMpc radius around the same quasar. Figure 1 shows the X-Shooter spectrum for J0148, displaying its Lyman alpha trough. In addition to the filters used in the survey done by Kashino et al. (2019), the g and Y bands have been included for this paper. We also make use of the z-band filter. The combined HSC data are summarized in Table 1.

Table 1: Summary of HSC Imaging in the J0148 field

Filter	t_{exp} (hrs)	Seeing	m_{PSF}	$m_{1.5"}$
g	2	0.75	26.1	26.1
$r2$	1.5	0.76	26.4	26.0
$i2$	2.4	0.8	26.0	25.6
$NB816$	4.5	0.73	25.2	25.0
z	6.2	0.82	25.2	25.1
Y	5.6	0.91	24.2	24.0

As noted by Christenson et al. (2021), the raw data was reduced with the LSST Science Pipeline, Version 21 (Ivezić et al. (2019); Jurić et al. (2015)). This process consists of combining CCDs into stacked mosaics using PanStarrs DR1 imaging (Chambers et al. (2016)) for astrometric and photometric calibrations. Furthermore, Source Extractor (Bertin and Arnouts (1996)) was used to identify the spatial coordinates of sources in the final stacked mosaics. Photometric measurements were then made at those positions based on PSF fitting.

The reason for using PSF fluxes is that the photometry is optimized to detect faint and unresolved sources for the purpose of constructing a density map. Christenson et al. (2021) outlines the photometry steps. Initially, each source position has a measured flux in a 1.5" aperture. The median sky background is then measured, excluding any pixels that are flagged by the data reduction pipeline as sources. Next, a 2-dimensional Gaussian profile is fit over a stamp of the combined mosaic 10 × 10" in size centered on the source. Each pixel is then analyzed. If a pixel differs by more than five times the noise in the sky background, it is excluded from the next iteration of fitting. This PSF measurement is conducted for all 6 bands, independently of one another. In the case for this paper, the PSF fluxes were used over the aperture fluxes as it allowed for detection of point-like sources.

II.II LBG Selection Procedure

The goal of this paper is to measure the presence of an overdensity or underdensity of galaxies relative to the position of the quasar. We will be examining LBGs in the redshift slice of $5.5 \leq z \leq 5.9$. In order to do this, the first step taken was applying a set of selection criteria onto the J0148 catalog. This step will help select the objects that fall in the redshift interval of interest. Albeit this sample will ultimately contain contaminates that will need to be further inspected. The process of how this was done will be discussed later.

The six bands used in this paper are g, r2, i2, NB816, z, and Y. The g-band filter covers a large expanse of the spectrum, going from UV all the way into visible light. The r2, i2, z, and Y bands follow suit, being more red filters respectively. The filter curves for these five bands can be seen in Figure 2. As for the NB816 filter, it is a narrowband filter. It's significance stems from the fact that it is sensitivite to LAEs within a narrow redshift range. However, it is not necessary to select LBGs. The reason for using the narrowband is because it was also used for the LAE selection done by Christenson et al. (2021). The filter curve for the narrowband can be seen in Figure 3.

LBGs in the redshift range of interest all have similar features in their spectrum. For higher redshift sources, we expect to see little to no transmittance in the bluer bands of g and r2, followed by a spike in flux somewhere in the i2-band. This is where the Lyman break is observed. A flattening of the flux should then be seen beyond into the z and Y bands. An example of this can be seen in Figure 4. This flattening in the z and Y bands is characteristic of LBGs as the flux should remain somewhat constant in the near-Infrared. This spectrum is observed to due the shorter wavelength light being absorbed by neutral Hydrogen, while the longer wavelength light is able to pass through. On the other hand, if an object is a low-redshift dusty galaxy, we expect to see little flux in the bluer bands as the dust absorbs much of the shorter wavelength radiation. This absorption is then followed by a rise in flux in the redder bands with no flattening into the Y-band.

In order to remove a large number of contaminants from the initial catalog, we require $\Delta F \leq 2\sigma_{\Delta F}$, with $\Delta F = |F_{PSF} - F_{ap}|$ and $\sigma_{\Delta F} = \sqrt{\sigma_{PSF}^2 + \sigma_{ap}^2}$, in all six bands. Doing this allows for the PSF flux measurements to be in a 2σ agreement with the corresponding aperture flux measurements. This is helpful as many of the PSF measurements contain contaminants that the aperture measurements do not contain. Applying this criteria reduced the number of sources in the J0148 catalog from 2,804,514 to 1,785,544.

Additional selection criteria were applied to the

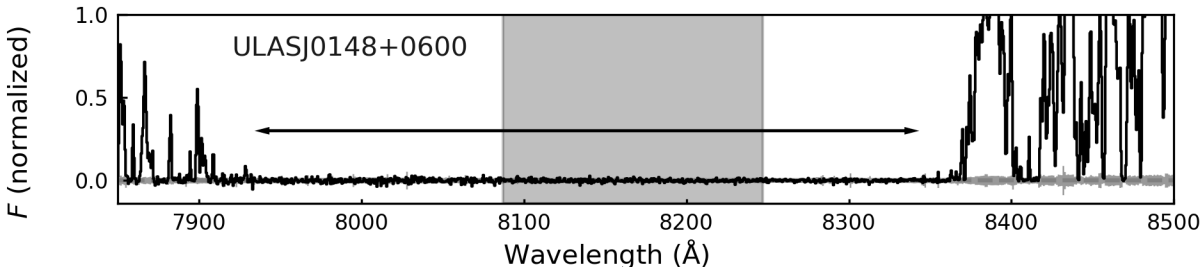

Figure 1: X-Shooter spectrum of ULAS J0148+0600, which exhibits a 110 h^{-1} Mpc Lyα trough with $\tau_{eff} \geq 7$ (Becker et al. (2015)). The extent of this trough is indicated by approximated by the black arrows. This quasar represents one of the most highly opaque sightlines known at z = 5.7. The region in gray represents wavelengths covered by the NB816 filter with at least 10% transmittance, which corresponds to Lyα at z $\simeq$ 5.7. Figure from Christenson et al. (2021).

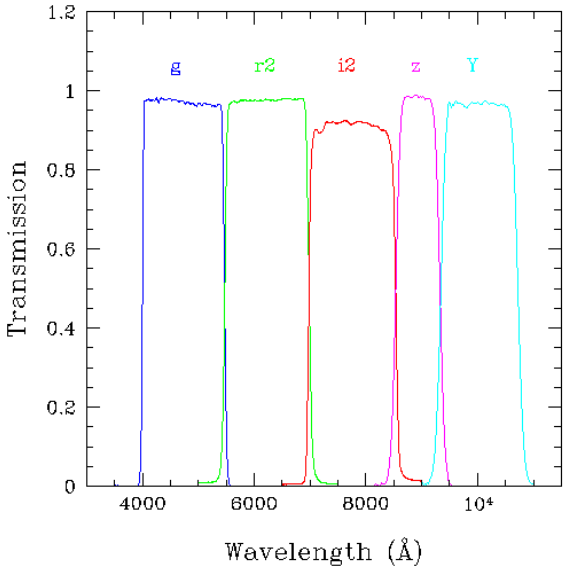

Figure 2: Transmittance for the g, r2, i2, z, and Y HSC filters. Figure from HSC.

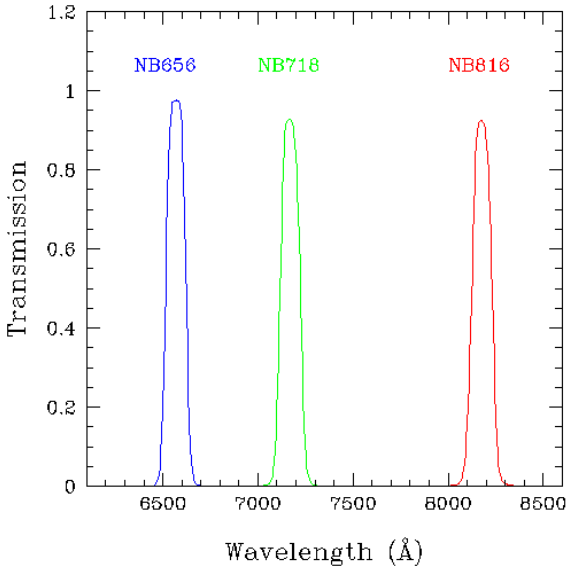

Figure 3: Transmittance for the NB816 filter in red. Figure from HSC.

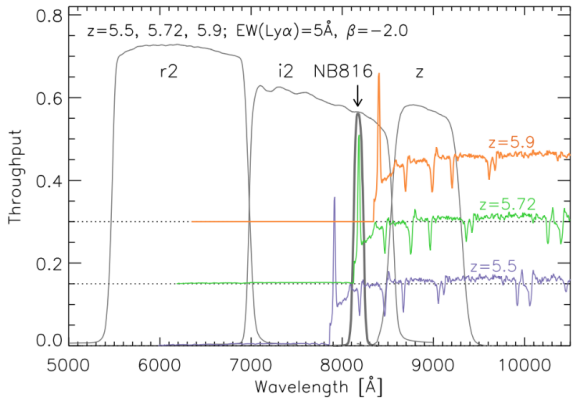

Figure 4: Transmittance of the HSC filters vs wavelength for the r2, i2, z, and NB816 bands. The LBG template spectra are shown with colored lines at z = 5.5, 5.72, and 5.9. The Lyman break can be seen occurring in the i2-band from the z-band. Figure from Kashino et al. (2019).

updated catalog to select LBGs for the redshift range of interest. All of these criteria are used to rule out low redshift objects. In order to select objects that are undetected in the r2 band, we require that the flux in the r2 band be less than or equal to 2σ. This will allow for us to remove lower redshift objects, because high redshift objects should not show up in the r2 band due to neutral hydrogen absorption. Although, if the source doesn't meet this criterion, then it must meet the criteria that the flux in the r2-band be greater than or equal to 2σ and the ratio between the flux in the i2-band and r2-band be greater than or equal to 2.5. This selection criteria also excludes low redshift objects because we expect the flux for high redshift objects to be mostly absorbed by the IGM at these wavelengths. Moreover, we require that the flux in the g-band be less than or equal to 2σ. This criterion further exludes low redshift sources.

Another criterion used in the selection of LBGs is limiting the dimness of the source in the z-band. We require that the magnitude in the z-band be less than or equal to 26.8. By doing this, we exclude sources that are too faint to get a high quality measurement.

In order to constrain the redshift, we require that the difference in magnitudes in the i2 and z bands be greater than or equal to 0.5. We point out these two bands in particular because this is where the Lyman break occurs at $5.5 \leq z \leq 5.9$. Applying this criterion will limit the i2-band flux to have a smaller measurement than the z-band flux. We see in Figure 5 that as the source becomes more redshifted (over roughly $4.8 < z < 6.0$), less and less of the galaxy light falls in the i2-band. The effect is pronounced because there is a sharp cutoff in the spectrum at a rest-frame of 1216 Å caused by IGM absorption blueward of Lyman-alpha. So, increasing the redshift means that this cutoff will fall increasingly redward. The i2-band spans rough 7000–8500 Angstroms, so the fraction of the filter subtended by the galaxy's flux will be sensitive to redshift over the range $z = \frac{7000\sim8500}{1216} - 1 = 4.8$ to 6.0. The z-band gives us a reference point for comparison, hence we use $i2 - z$. For a source over this redshift range, the z-band also tells us roughly what the rest-frame UV luminosity is. Sources that didn't meet this selection criterion can also be seen in Figure 5. The objects that we're selecting are from a fairly small region of color-magnitude space. Additionally, we require the z-band flux be greater than or equal to 5σ. Meaning, we only allow sources in which we are highly confident in being a real source of flux, ruling out pixels and background fluctuations.

To summarize, the final selection criteria applied to our LBGs are as follows:

- $F_{r2} \leq 2\sigma_{r2}$ or $F_{r2} \geq 2\sigma_{r2}$ and $\frac{F_{i2}}{F_{r2}} \geq 2.5$
- $F_g \leq 2\sigma_g$
- $z_{AB} \leq 26.8$
- $(i2 - z)_{AB} > 0.5$
- $F_z \geq 5\sigma_z$

Applying these criteria narrows our selection catalog from 1,785,544 objects to 2,502 objects.

II.III Photometric Redshifts

Next, each source that passes these criteria goes through a photometric redshift code, EAZY, to determine the redshifts of these objects as well as the probability density function (PDF) of their attributed redshift. This step will continue to remove sources that are outside the redshift range of interest.

EAZY is a photometric redshift code by Brammer et al. (2008) that is designed to produce high-quality redshift estimates for situations where spectroscopic redshifts are not available. Details of the algorithm and tests of the code are presented by Brammer et al. (2008). We use EAZY to determine redshifts for the sources in our catalog and their probabilities of being at said redshift.

The parameters used for EAZY will be outlined here. First, we assume the reddening caused by the Milky Way is 0. We also set any extra corrections for reddening to False. For the redshift grid, we

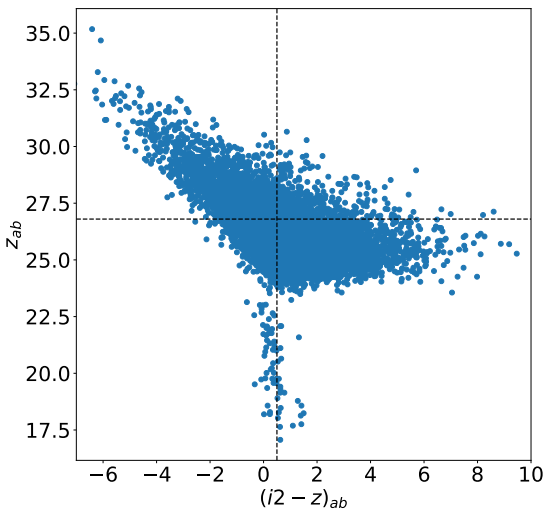

Figure 5: A distribution of objects from the J0148 catalog showing their respective $(i2-z)_{AB}$ and z_{AB} magnitudes. The vertical dashed line represents the selection criterion $(i2-z)_{AB} > 0.5$. The horizontal dashed line represents the selection criterion $z_{AB} \leq 26.8$. The area in the bottom right corner shows the small sample of objects that are being selected.

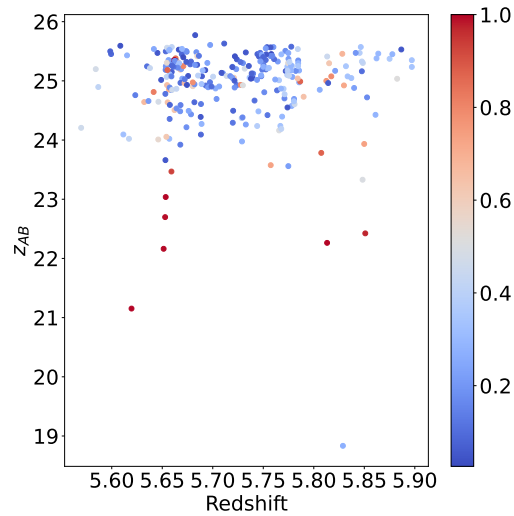

Figure 6: All 266 LBG candidates plotted with their z magnitudes as a function of their photometric redshifts. The colorbar on the right refers to the confidence level for each object in the redshift range of interest.

set the minimum to 0.01, maximum to 10, and the step to 0.01. No prior was applied to the objects in our catalog. Instead of opting for the default template file provided by EAZY, we used a template file from Larson et al. (2022). This file included the FSPS template provided by Brammer et al. (2008) as well as two BPASS models included by Larson et al. (2022). Larson et al. (2022) notes that these are useful for galaxies at high z where Lya is attenuated by neutral IGM. Furthermore, using these templates proved to be helpful for selecting dim objects as the default template provided by Brammer et al. (2008) had a bias for brighter objects.

Now, we find the redshift for each object in our catalog. EAZY does this by finding the maximum likelihood redshift over the entire grid. The likelihood of each object's redshift is given as a log-likelihood. This probability distribution spans the entire redshift grid, with the highest probability being at the maximum likelihood redshift. We set our boundaries so that EAZY only returns objects that have peaks in the redshift range of interest. By doing this step, we trim the number of sources in our catalog from 2,502 to 873. Furthermore, we calculate the area under the probability curve in the redshift range $5.5 \leq z \leq 5.9$ to determine the level of confidence we have for each of these objects given this redshift range.

III Results and Analysis

For the final step of the LBG selection, we visually inspected each of 873 sources to reject any hot pixels, cosmic rays, moving objects, and any other extraneous objects. This step was done by analyzing the cutout images in each of the six bands as well as the photometric SEDs. Further explanation will be provided later. Using this procedure, we select 266 LBGs in the J0148 field, 81 more than presented in Kashino et al. (2019).

We gain a better understanding of certain properties of the LBGs in the field by plotting their z magnitude vs redshift shown in Figure 6, color coded by their confidence level. There tends to be a clustering of objects around the redshift range of 5.65 to 5.8. These are also very faint objects in the z-band, with most of the sources being low confidence.

We see an agreement with this finding in Figure 7, showing the redshift vs probability, with each object color coded by their z magnitudes. However, in this plot we see a clustering of objects of higher confidence levels closer to the $z = 5.65$ boundary and less so at higher redshifts. This shouldn't be a surprise however as we expect there to be a slight bias towards closer sources. Additionally, Figure 8 shows an agreement with these findings as well, showing the z magnitude of these objects vs their probability.

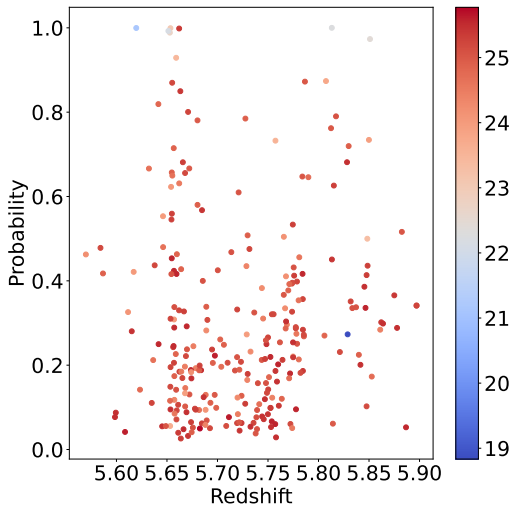

Figure 7: All 266 LBG candidates plotted with their confidence level as a function of their photometric redshifts. The colorbar on the right refers to the z magnitude for each object in the redshift range of interest.

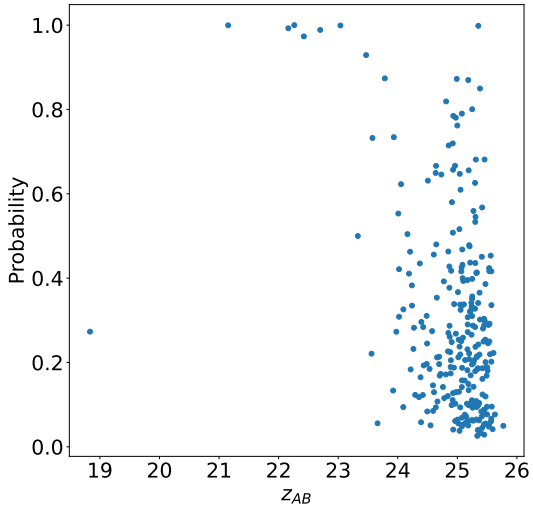

Figure 8: All 266 LBG candidates plotted with their confidence level as a function of their z magnitudes.

We now turn to the combined results of the photometric selection and redshift. Cutout images for example LBG candidates selected are shown in Figure 9, alongside their respective photometric SED fit and PDF. Additionally, examples of objects that are considered contaminants are shown in Figure 10. Each of the cutout images show an example candidate in each of the six filters used: g, r2, i2, NB816, z, and Y. Furthermore, Each cutout image is 10" on each side and is centered on the LBG candidate. In Figure 9, the examples chosen were to demonstrate the confidence level of each object in the redshift range of interest. The first row being an example of an object with high confidence ($\sim$ 68%), the second being an object with medium confidence ($\sim$ 50%), and the third being an object with low confidence ($\sim$ 20%). The examples in Figure 10 were chosen to demonstrate contaminants that show up frequently. The first row being an example of a hot pixel, the second being a low-redshift dusty object, and the third being an example of a non-detection.

The spatial distribution of LBGs in the J0148 field at two different confidence levels is shown in Figure 11. In the first panel, we see all 266 LBG candidates color coded by their z magnitudes. Some structure can be seen, but at a confidence level greater than 0%, it appears to be more so of a random distribution of objects. In the second panel, we set the limit of the confidence level to greater than 80%, but only 5 objects can be seen. This number is too small to make any proper conclusion on the field.

In Figure 12, the spatial distribution of LBGs is shown with 50% confidence or more of each source in the range $5.5 \leq z \leq 5.9$. By setting 50% as our minimum confidence level, we select 29 LBGs in the field. We chose this as the cutoff for the confidence level as it allows for some structure to be seen without overpopulating the density map with low confidence objects. The panel on the left has a spatial distribution of the LBGs shown with their colors corresponding to their z-magnitudes, the top right with their colors corresponding to their redshift, and the bottom right corresponding to their probability of lying within the redshift range of interest. The quasar is centered in each panel and denoted with a star. Dotted concentric circles are plotted in increments of 8'. Table 2 summarizes the properties of the 29 LBGs in the J0148 field. We count the number of objects in each 8' bin. This data can be seen in Table 3.

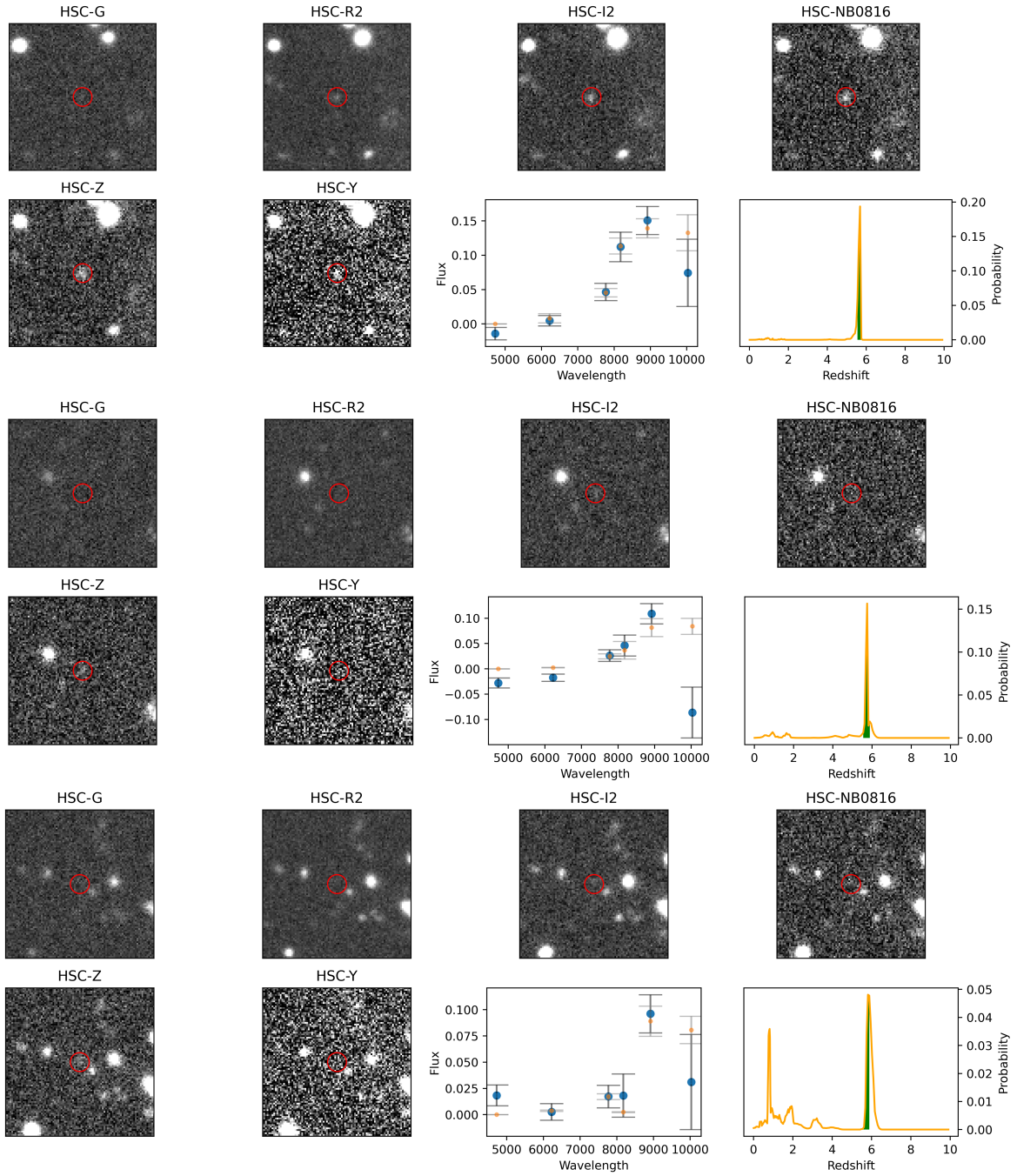

Figure 9: Example LBG candidates in the J0148 field. The first six images in each row shows the object in each of the six filters. Each row demonstrates an object with confidence levels $\sim 68\%$, $\sim 50\%$, and $\sim 20\%$ respectively. The flux [μJy] vs wavelength[Å] graph displays the measured flux for each band in blue and the model flux estimated by EAZY in orange. The probability vs redshift plot displays the PDF of the object over the redshift grid $0.1 < z < 10$. Colored in green is the probability of the object in the redshift range $5.5 \leq z \leq 5.9$.

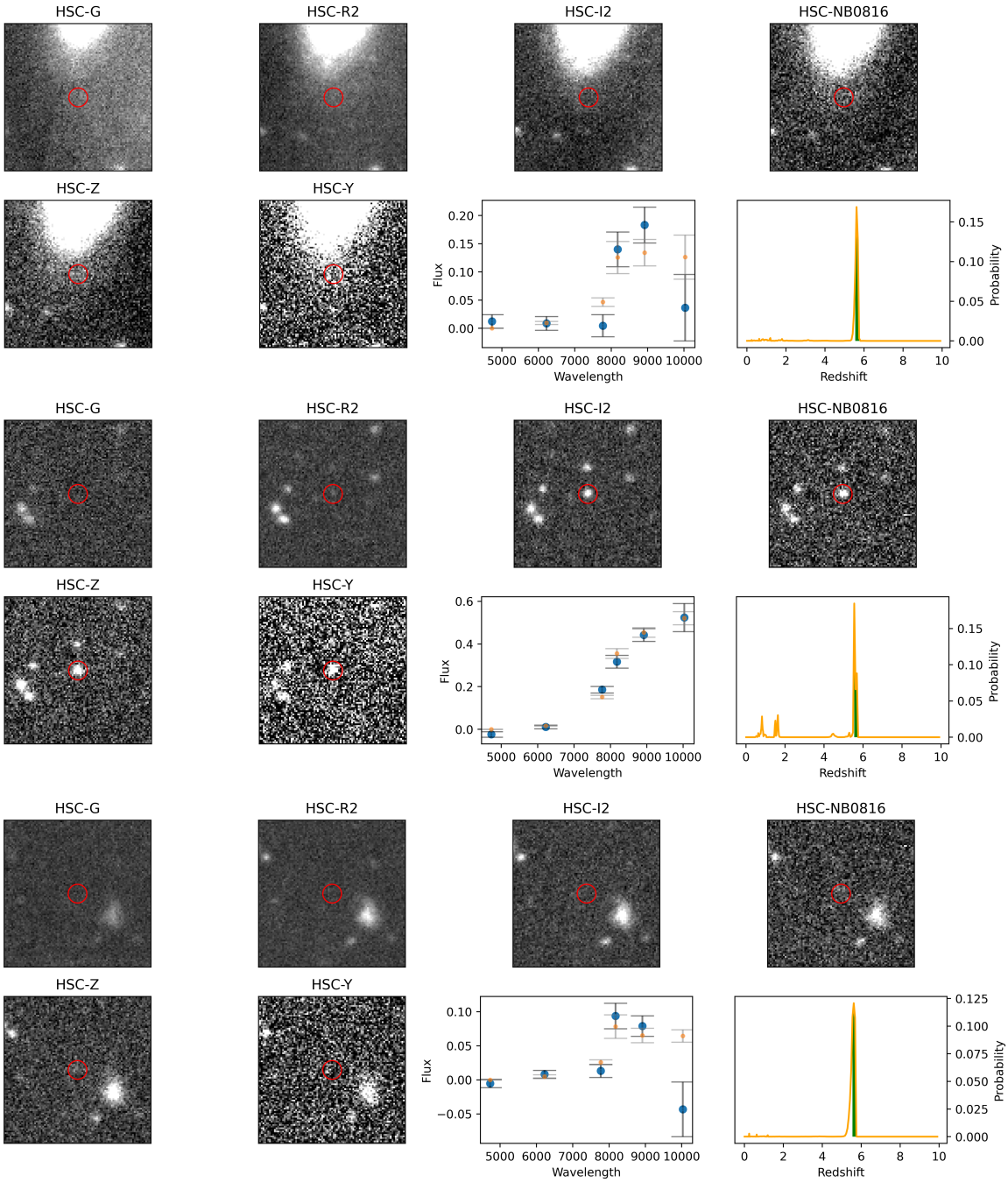

Figure 10: Example contaminants found in the J0148 field. The first row demonstrates a hot pixel. The second row demonstrates a dusty low-redshift object. The third row demonstrates a non-detection. Each passed the photometric redshift selection and needed to be disregarded through a visual inspection.

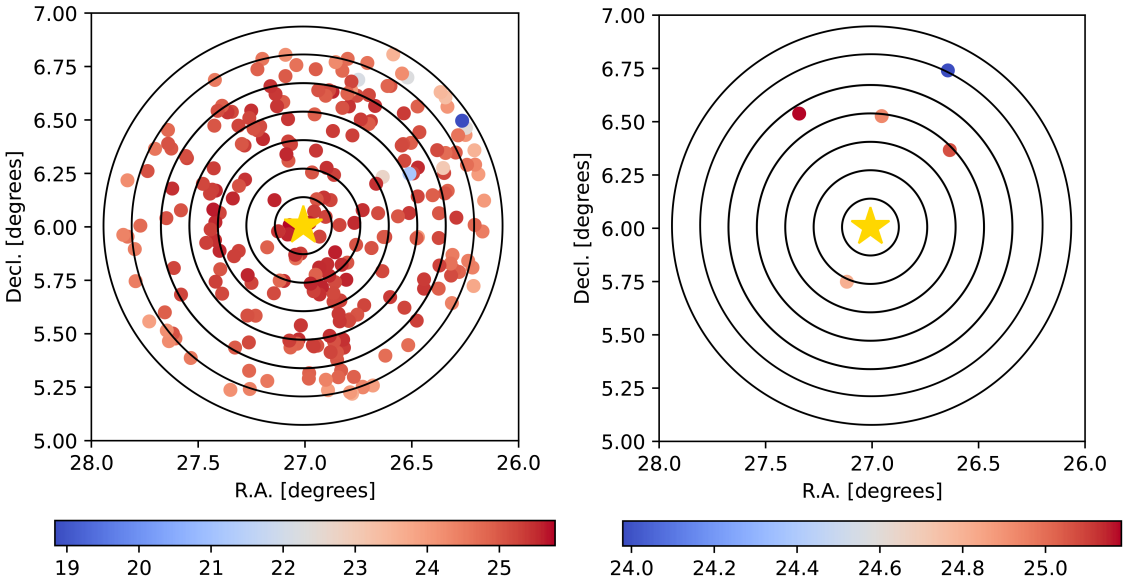

Figure 11: Distribution of all LBG candidates (left), and LBG candidates with 80% or higher confidence (right). Each color coded by their z-band magnitude. Concentric circles are shown in increments of 8' from the quasar.

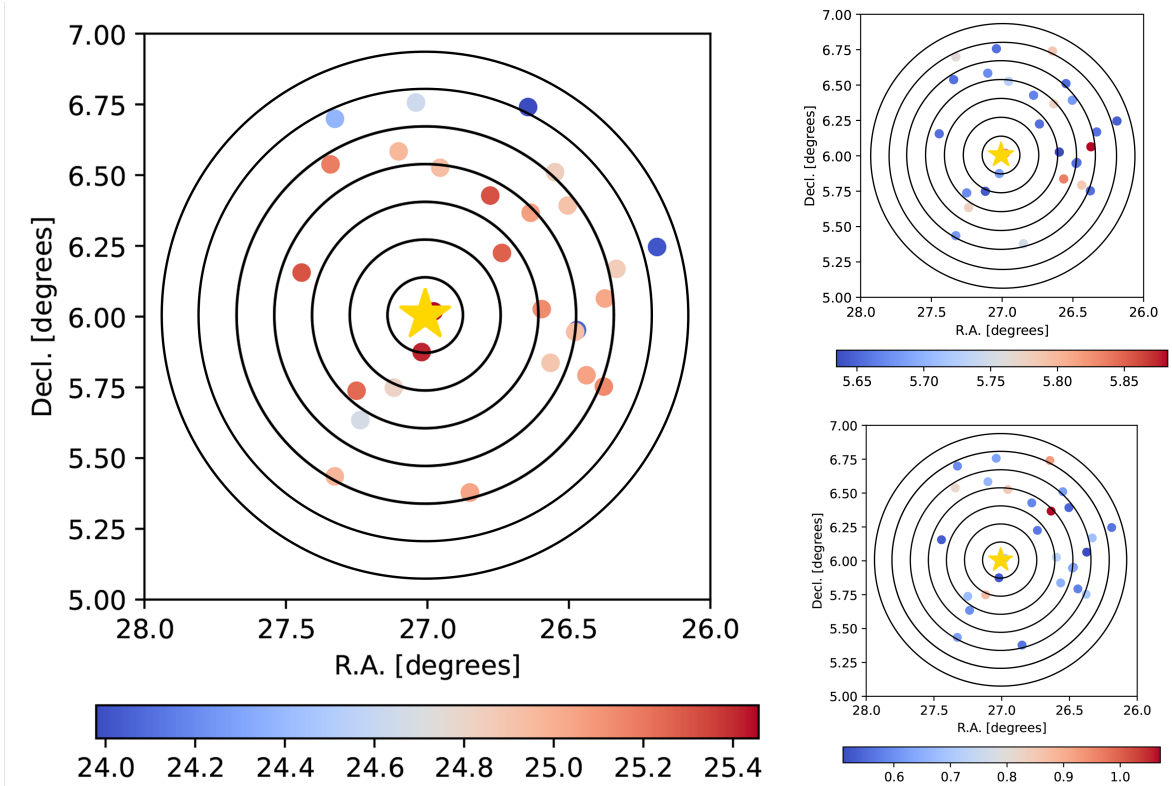

Figure 12: Distribution of LBG candidates with 50% or higher confidence level color coded by their z-magnitudes (left), redshift (top right), and confidence level (bottom right). Concentric circles are shown in increments of 8' from the quasar.

Table 2: Summary of LBGs

RA	Dec	z	m_z
26.18829788	6.2460558	5.64606762	24.00950880
26.33190797	6.1686528	5.65670300	24.85480907
26.37666045	5.7526640	5.65420151	25.14132621
26.37276423	6.0639311	5.88251019	25.03523171
26.43788951	5.7928147	5.78570127	25.05496609
26.47128094	5.9523570	5.65406704	24.05515106
26.47761968	5.9462952	5.65475702	24.92852331
26.50414718	6.3927176	5.68024683	24.90990310
26.56491172	5.8366895	5.83572006	24.89178955
26.54900121	6.5103997	5.65371132	24.84352307
26.59593228	6.0266535	5.63468838	25.13551092
26.63517236	6.3669751	5.77697754	25.06979192
26.64419708	6.7406171	5.78583050	23.97909621
26.73651515	6.2249147	5.65467072	25.26725458
26.77798380	6.4277647	5.66573715	25.31040760
26.84970075	5.3781668	5.72092199	25.05371019
26.84987846	5.4115469	5.74766159	25.04565226
26.97786336	6.0184699	5.82823515	25.45716291
26.95489442	6.5261883	5.72763968	24.93198321
27.02035991	5.8746777	5.68468666	25.41569898
27.04038637	6.7567002	5.65531874	24.63625380
27.11843442	5.7490181	5.64149380	24.81186718
27.10168783	6.5838235	5.67208576	24.96118878
27.23715379	5.6342314	5.77546787	24.67210958
27.25042904	5.7379867	5.67091131	25.24888435
27.32743928	5.4353444	5.68022013	24.97401654
27.32681844	6.6991412	5.76269054	24.37412301
27.34245745	6.5380791	5.65516424	25.18323379
27.44459483	6.1556291	5.65445948	25.30539041

Table 3: LBG Number Density in J0148 ($\geq 50\%$)

R (arcminutes)	N_{LBGs}
4(0-8)	1
12 (8-16)	2
20 (16-24)	3
28 (24-32)	7
36 (32-40)	9
44 (40-48)	7

Our results are consistent with the results presented in Kashino et al. (2019). Figure 12 shows a pronounced underdensity within 8' ($\sim$ 19 cMpc) of the quasar position that Kashino et al. (2019) reports. However, by limitng the confidence level for each object to be 50 percent or greater, we see an underdensity going farther out into 16' of the quarsar position. We find only one candidate within 8' of the quasar sightline, and three within 16', or roughly one third of the background density. This is a demonstration that the extreme Gunn-Peterson trough towards J0148 is related with a region of highly underdense LBGs. Comparing our density to the one presented in Kashino et al. (2019), we see a correlation of the distribution of LBGs and the structures they are probing.

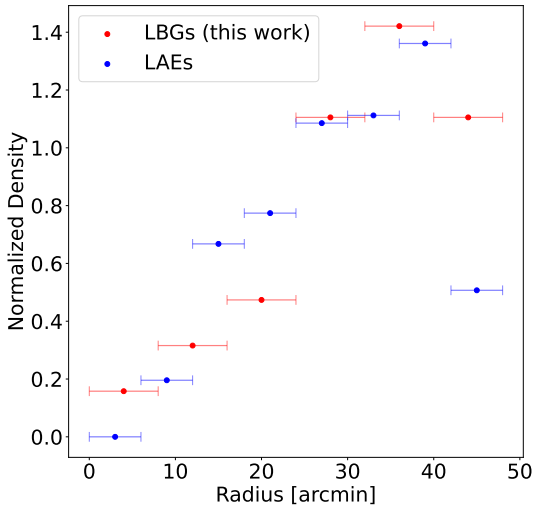

Figure 13: Surface density of LBGs versus LAEs in the J0148 field normalized by the mean density between $\sim$15' to $\sim$40'(outside the center of the field) of the respective surveys. The red lines indicate the size of the radius bin of our work, while the blue lines indicate the radius bin in Christenson et al. (2021).

We now compare the results found here to the updated selection of LAEs done by Christenson et al. (2021) in the J0148 field. By comparing our density map to the one presented by Christenson et al. (2021) by eye, we found little to no similarities between structures that the LAEs and the LBGs are probing. As a matter of fact, there seems to be voids in the density of LBGs where an overdensity of LAEs are. Given the data we have, it is inconclusive whether or not this mismatch has a relation or if it's just a mere coincidence. However, the underdensity of LBGs within 20 h^{-1} Mpc is in agreement with the underdensity of LAEs presented in Christenson et al. (2021). In Figure 13, we over plot the LAE surface density profile taken from Christenson et al. (2021). The radial profiles of the LBG and LAE samples are in agreement, following a trend of the number of sources increasing further away from the quasar.

We note that providing a more quantitative analysis is difficult given that this study has only been done over one field. However, because the redshift window for LBGs is as wide as the length of the J0148's trough, these results further strengthen the presence of an exceptionally long region that is highly underdense along the quasar sightline. This could be a single void that expands along the entire length of the trough, or multiple voids that overlap

in projection.

IV Summary

We have conducted a search for Lyman break galaxies at 5.5$\leq z \leq$ 5.9 in the field of the $z = 6$ quasar ULAS J0148+0600, whose spectrum shows an extremely elongated and opaque Lyα absorption trough in the relevant redshift range. Our goal was to establish the density of LBGs in highly opaque quasar sightlines, such as the one seen in J0418. If there appears to be a normal distribution of galaxies within the vicinity of the opaque quasar sightline, then this would point to LAEs not being a reliable source for probing surface density. However, if LBGs are shown to have a scarcity within the vicinity of the opaque quasar sightline, then this could point to evidence for reionization lasting later than $z = 6$.

We have constructed a catalog of 29 highly confident LBG candidates within 56' of the quasar position. The color criteria used were optimized for finding LBGs within the redshift slice of 5.5$\leq z \leq$ 5.9. Additionally, we used the photometric redshift code EAZY to obtain high quality redshifts for these sources. The spatial distribution of these objects shows an apparent deficiency within $\sim$ 16' of the quasar's position. This result confirms the lack of LBGs presented in Kashino et al. (2019), while further emphasising an LBG scarcity in the field.

Comparing our results to the LAE survey done by Becker et al. (2018)(Christenson et al. (2021)), we see an agreement with the normalized surface density of sources as a function of distance. This correlation suggests that the lack of LAEs in the vicinity of the quasar sightline presented in Becker et al. (2018) is not purely due to Lyman-alpha emission suppression due to the high opacity, but rather a true deficiency of galaxies. Moreover, our catalog of LBG candidates covers the full length of the trough that were measured in six different filters, instead of a narrow redshift range probed by the LAEs in a narrowband filter and LBGs in just the r2, i2, and z filters, suggesting a spatially consistent underdensity associated with the trough.

In order to make more conclusive statements, further observations in multiple quasar fields would be required. Christenson et al. (2021) presents an undersdensity of LAEs in the quasar SDSS J1250+3130 ($\tau_{eff} \geq 6$). A survey of LBGs performed in this field would further help to determine whether or not it is fair to use LAEs our main probe of density in opaque quasar sightlines. Using photometric redshifts to select candidates in our redshfit range of interest proved to be useful as a means for providing accurate data for high redshift galaxies and should continue to be tested for future surveys.

References

Houjun Mo, Frank C. van den Bosch, and Simon White. *Galaxy Formation and Evolution*. 2010.

Bradley W. Carroll and Dale A. Ostlie. *An Introduction to Modern Astrophysics*. 2nd (international) edition, 2007.

Xiaohui Fan, Michael A. Strauss, Robert H. Becker, Richard L. White, James E. Gunn, Gillian R. Knapp, Gordon T. Richards, Donald P. Schneider, J. Brinkmann, and Masataka Fukugita. Constraining the Evolution of the Ionizing Background and the Epoch of Reionization with z~6 Quasars. II. A Sample of 19 Quasars. , 132(1): 117–136, July 2006. doi: 10.1086/504836.

Girish Kulkarni, Laura C Keating, Martin G Haehnelt, Sarah E I Bosman, Ewald Puchwein, Jonathan Chardin, and Dominique Aubert. Large Ly α opacity fluctuations and low CMB τ in models of late reionization with large islands of neutral hydrogen extending to z
lt; 5.5. *Monthly Notices of the Royal Astronomical Society: Letters*, 485(1):L24–L28, 02 2019. ISSN 1745-3925. doi: 10.1093/mnrasl/slz025. URL https://doi.org/10.1093/mnrasl/slz025.

Holly M. Christenson, George D. Becker, Steven R. Furlanetto, Frederick B. Davies, Matthew A. Malkan, Yongda Zhu, Elisa Boera, and Adam Trapp. Constraints on the end of reionization from the density fields surrounding two highly opaque quasar sightlines. *The Astrophysical Journal*, 923(1):87, dec 2021. doi: 10.3847/1538-4357/ac2a34. URL https://doi.org/10.3847/1538-4357/ac2a34.

George D. Becker, Frederick B. Davies, Steven R. Furlanetto, Matthew A. Malkan, Elisa Boera, and Craig Douglass. Evidence for large-scale fluctuations in the metagalactic ionizing background near redshift six. *The Astrophysical Journal*, 863(1):92, aug 2018. doi: 10.3847/1538-4357/aacc73. URL https://doi.org/10.3847/1538-4357/aacc73.

George D. Becker, James S. Bolton, and Adam Lidz. Reionisation and high-redshift galaxies:

The view from quasar absorption lines. *Publications of the Astronomical Society of Australia*, 32:e045, 2015. doi: 10.1017/pasa.2015.45.

Daichi Kashino, Simon J. Lilly, Takatoshi Shibuya, Masami Ouchi, and Nobunari Kashikawa. Evidence for a highly opaque large-scale galaxy void at the end of reionization. *The Astrophysical Journal*, 888(1):6, dec 2019. doi: 10.3847/1538-4357/ab5a7d. URL https://doi.org/10.3847/1538-4357/ab5a7d.

Željko Ivezić, Steven M. Kahn, J. Anthony Tyson, Bob Abel, and et al. Acosta. LSST: From Science Drivers to Reference Design and Anticipated Data Products. , 873(2):111, March 2019. doi: 10.3847/1538-4357/ab042c.

Mario Jurić, Jeffrey Kantor, and et al. Lim. The lsst data management system, 2015. URL https://arxiv.org/abs/1512.07914.

K. C. Chambers, E. A. Magnier, and et al. Metcalfe, N. The pan-starrs1 surveys, 2016. URL https://arxiv.org/abs/1612.05560.

E. Bertin and S. Arnouts. SExtractor: Software for source extraction. , 117:393–404, June 1996. doi: 10.1051/aas:1996164.

Gabriel B. Brammer, Pieter van Dokkum, and Paolo De Coppi. Eazy: A fast, public photometric redshift code. *The Astrophysical Journal*, 686:1503–1513, 2008.

Rebecca L. Larson, Steven L. Finkelstein, Taylor A. Hutchison, Casey Papovich, Micaela Bagley, Mark Dickinson, Sofía Rojas-Ruiz, Harry C. Ferguson, Intae Jung, Mauro Giavalisco, Andrea Grazian, Laura Pentericci, and Sandro Tacchella. Searching for islands of reionization: A potential ionized bubble powered by a spectroscopic overdensity at z = 8.7. *The Astrophysical Journal*, 930(2):104, may 2022. doi: 10.3847/1538-4357/ac5dbd. URL https://doi.org/10.3847/1538-4357/ac5dbd.

Appendix

Comparison of density maps to Kashino et al. (2019) and Christenson et al. (2021)

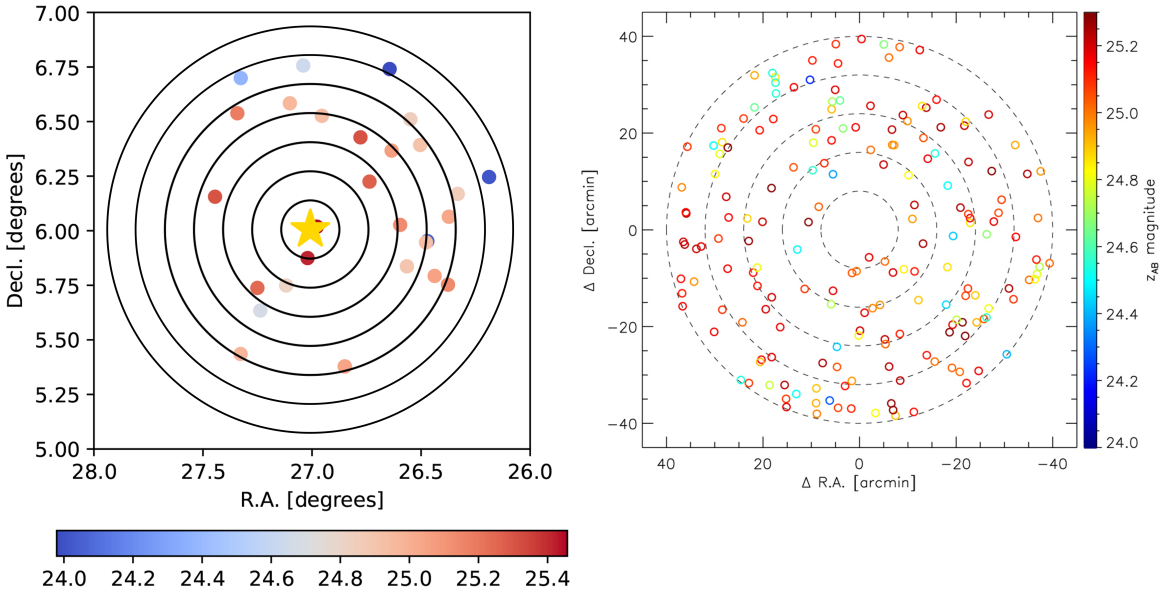

Figure 14: The density map of LBGs from this paper (left) compared to the map presented in Kashino et al. (2019) (right).

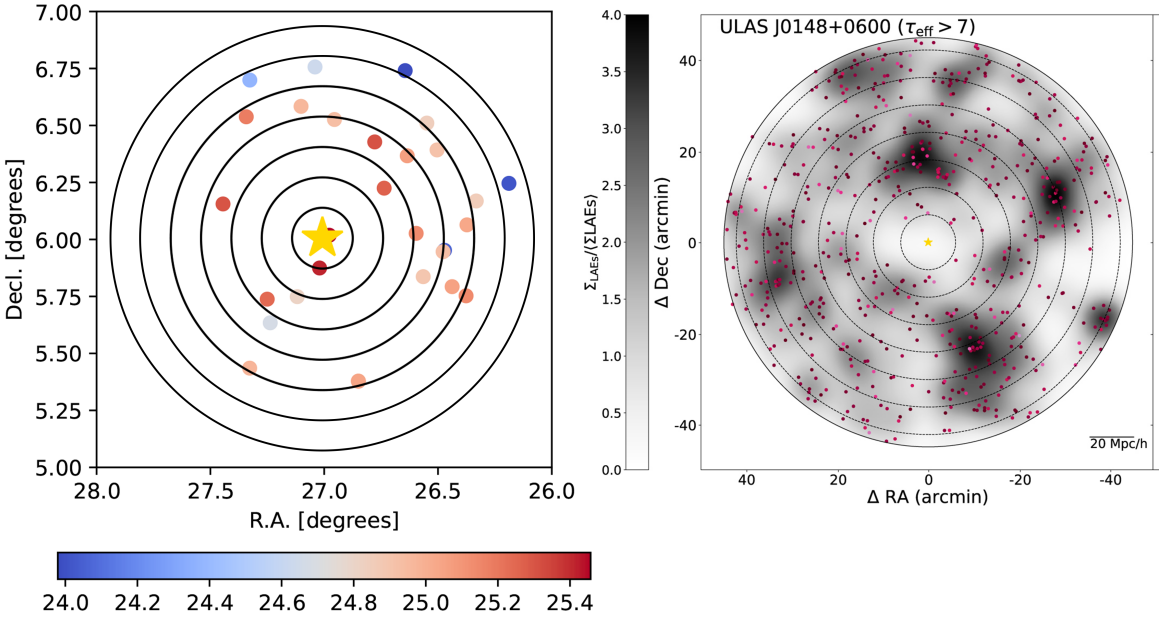

Figure 15: The density map of LBGs from this paper (left) compared to the density map of LAEs presented in Christenson et al. (2021) (right).